Heliyon 10 (2024) e23527

Contents lists available at ScienceDirect

Heliyon

journal homepage: www.cell.com/heliyon

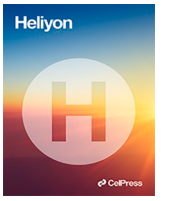

Effect of quercetin-loaded poly (lactic-co-glycolic) acid nanoparticles on lipopolysaccharide-induced memory decline, oxidative stress, amyloidogenesis, neurotransmission, and Nrf2/HO-1 expression

Rasha M. Hussein [a,b,*], Mohamed A. Kandeil [c], Hatem M. Soliman [a], Ahmed A.G. El-Shahawy [d]

[a] Department of Biochemistry, Faculty of Pharmacy, Beni-Suef University, Beni-Suef, Egypt
[b] Department of Pharmaceutics and Pharmaceutical Technology, Faculty of Pharmacy, Mutah University, Al-Karak, Jordan
[c] Department of Biochemistry, Faculty of Veterinary Medicine, Beni-Suef University, Beni-Suef, Egypt
[d] Materials Science and Nanotechnology Department, Faculty of Postgraduate Studies for Advanced Sciences (PSAS), Beni-Suef University, Egypt

ARTICLE INFO

Keywords:
Quercetin
Antioxidant
Nanoparticles
Brain
Amyloid beta

ABSTRACT

Neuroinflammation contributes to the pathogenesis of several neurodegenerative disorders. This study examined the neuroprotective effect of quercetin (QUR)-loaded poly (lactic-co-glycolic) acid (PLGA) nanoparticles (QUR NANO) against the neurotoxicity induced by lipopolysaccharide (LPS) in mice. A QUR NANO formulation was prepared and characterized by differential scanning calorimetry, X-ray diffraction, entrapment efficiency (EE), high-resolution transmission electron microscopy, field emission scanning electron microscopy, and *in vitro* drug release profile. Levels of glutathione, malondialdehyde, catalase, inducible nitric oxide synthase (iNOS), amyloid beta 42 ($A\beta_{42}$), β-secretase, gamma-aminobutyric acid (GABA), and acetylcholine esterase (AChE) were measured in the mouse brain tissues. The gene expression of nuclear factor erythroid-related factor 2 (*Nrf-2*) and heme oxygenase-1 (*HO-1*) were also determined. The prepared QUR NANO formulation showed 92.07 ± 3.21% EE and drug loading of 4.62 ± 0.55. It exhibited clusters of nano-spherical particles with smooth surface areas, and the loading process was confirmed. *In vivo*, the QUR NANO preserved the spatial memory of mice and protected the hippocampus from LPS-induced histological lesions. The QUR NANO significantly reduced the levels of malondialdehyde, iNOS, $A\beta_{42}$, β-secretase, and AChE in brain tissue homogenates. Conversely, QUR NANO increased the glutathione, catalase, and GABA concentrations and upregulated the expression of *Nrf-2* and *HO-1* genes. Remarkably, the neuroprotective effect of QUR NANO was significantly greater than that of herbal QUR. In summary, the prepared QUR NANO formulation was efficient in mitigating LPS-induced neurotoxicity by reducing memory loss, oxidative stress, and amyloidogenesis while preserving neurotransmission and upregulating the expression of *Nrf2* and *HO-1* genes. This study addresses several key factors in neuroinflammatory disorders and explores the potential of QUR-loaded nanoparticles as a novel therapeutic approach to alleviate these factors.

* Corresponding author. Department of Biochemistry, Faculty of Pharmacy, Beni-Suef University, Salah Salem Street, 62514, Beni-Suef, Egypt.
E-mail address: rasha.hussein@pharm.bsu.edu.eg (R.M. Hussein).

https://doi.org/10.1016/j.heliyon.2023.e23527
Received 14 August 2023; Received in revised form 11 November 2023; Accepted 5 December 2023
Available online 10 December 2023

1. Introduction

Neuroinflammation is recognized as a severe public health concern. It is commonly induced by toxic metabolites, microbes, brain trauma, spinal cord injury, autoimmunity, or aging [1]. Particularly, lipopolysaccharide (LPS), found at the cell wall of gram-negative bacteria, serves as a potent stimulator of the immune system. LPS activation in the brain triggers the expression of inflammatory cytokines, resulting in neuroinflammation and neurodegeneration [2]. Furthermore, the oxidative stress caused by the overproduction of reactive oxygen species (ROS) leads to the formation of amyloid beta 42 ($A\beta_{42}$) peptides, a hallmark of neurodegenerative diseases like Alzheimer's disease (A.D.) [3].

One of the central protective mechanisms against neuronal oxidative stress is the activation of nuclear factor erythroid 2-related factor 2 (Nrf2), which controls the expression of several detoxifying, antioxidant, and anti-inflammatory genes [4,5]. Dysregulated Nrf2 activity has been reported in both human and animal A.D. brains, confirming its role in memory function and amyloidogenesis [6]. Quercetin (QUR), a natural polyphenol flavonoid, has shown neuroprotective properties by counteracting oxidative stress and modulating survival pathways in the cell [7,8]. Nevertheless, QUR encounters some limitations such as low solubility and bioavailability, resulting in its rapid degradation and therefore, the need for longer treatment periods or higher concentrations [9].

To solve these limitations, nanotechnology has been suggested to design QUR-loaded nanoparticles (QUR NANO) using poly (lactic-co-glycolic) acid (PLGA) polymers. PLGA shows a high encapsulation efficacy, biodegradable, biocompatible, and stable properties [10]. These characteristics enable controlled drug release, improving solubility and bioavailability.

The current research has the potential to improve drug delivery techniques, advance therapeutic development, and enhance strategies for protecting the nervous system from neuroinflammation and related disorders by investigating the advantages of the QUR NANO formulation. Our study aims to investigate whether the newly designed QUR NANO formulation has a neuroprotective effect compared to the herbal QUR and what are the effects of QUR NANO formulation on memory function, oxidative stress, amyloid buildup, and disruption of neurotransmission induced by LPS in mice?

2. Materials and methods

2.1. Materials

Quercetin (M.Wt.: 302.23 Da), PLGA (75:25, M.Wt.: 66,000–10,700 Da), and endotoxin lipopolysaccharide (LPS, gram-negative bacteria, *Escherichia coli*) were obtained from Sigma-Aldrich Chemicals Co. (USA). Propylene carbonate, polyvinyl alcohol (PVA, M. Wt.: 30,000–70,000 Da), luminol, and absolute ethanol (99.5–99.8%) were bought from Aldrich Chemical Co. (USA).

2.2. Preparation of PLGA N.P.s and QUR NANO

QUR in nano form was prepared using the nanoprecipitation method [11]. Briefly, a solution of 5 mg/ml QUR in ethanol was added to deionized water at a volume ratio of 1:35 under magnetic stirring (2000 rpm) at a fixed flow rate (10 ml/min). The QUR N.P.s were then filtered and dried under a vacuum.

PLGA N.P.s were prepared by the method of emulsification diffusion [12]. Briefly, a mixture of 200 mg PLGA, 10 ml of propylene carbonate (P.C.) solvent, and 10 ml of an aqueous solution having PVA stabilizer was emulsified for 15 min using a high-speed homogenizer. Under magnetic stirring, 80 ml of water was mixed with the oil: water emulsion to destabilize the equilibrium, diffuse the P. C. solvent into the water phase, and precipitate the PLGA N.P.s. The P.C. was removed by dialysis, and the PLGA was lyophilized. To formulate QUR NANO, 30 mg of QUR in nano form was added during the initial step of PLGA N.P.s formation, followed by the same procedure as mentioned above.

2.3. Characterizations study

2.3.1. Determination of the entrapment efficiency and drug loading capacity

The entrapment efficiency (EE) of QUR nanoparticles was assessed by centrifugating samples at 10,000 rpm for 20 min at 25 °C. The quantity of entrapped drug within nanoparticles was estimated by Equation (1). The non-entrapped QUR in the supernatant was determined by HPLC analysis according to Ref. [13]. The EE and drug-loading (DL) of QUR in the nanoparticles were calculated by:

$$\text{QUR (EE)} = \text{Amount of QUR originally taken} - \text{Amount of QUR in supernatant/Amount of QUR originally taken} * 100 \quad (1)$$

$$\text{QUR (DL)} = \text{Amount of QUR originally taken/Amount of NPs loaded with QUR} * 100 \quad (2)$$

2.3.2. Crystallinity and morphology determination

The crystallinity was determined using X-ray diffraction (XRD, PANalytical Empyrean) with Cu Kα radiation ($\lambda = 0.154\ cm^{-1}$), a scan angle of 5–80, a current of 35 mA, and an accelerating voltage of 40 kV. The scan was set to 0.04. The structure and morphology were studied using high-resolution transmission electron microscopy (H-RTEM) and field emission scanning electron microscopy (FESEM) (JOEL JEM-2100) with 200 kV of acceleration voltage. The thermal performance of the samples was evaluated by differential scanning calorimetry (DSC) using a Shimadzu DSC-60 instrument (Japan). The DSC curves were prepared by aluminum crucibles with

a 5 mg sample under 20 ml/min of dynamic air atmosphere at a heating rate of 10 °C/min. The program used for scanning was isothermal for 1 min at −20 °C and scanning from −15 °C to 600 °C at a 10 °C/min scanning rate. After scanning the sample three times, the mean plus S.D. for the melting point (°C) and the energy used (D) in the melting process (J/g) were calculated.

2.3.3. In vitro drug release

The *In vitro* release of QUR-PLGA nanoparticles was performed by dispersing 10 mg equivalent QUR in 10 ml of 100 mM phosphate buffer (pH 7.4) in a 50 ml volumetric flask and incubated at 37 °C in a shaker water bath. Half ml aliquots were withdrawn in vials from the release medium and replaced with fresh buffer medium at predetermined time intervals of 0, 1/2, 1, 2, 3, 6, 8, 12, and 24 h. The amount of released QUR/timed sample was determined by HPLC. A standard curve was constructed, considering the dilution factor.

2.4. In vivo study

2.4.1. Animals

Seventy male BALB/c mice weighing 26.5–32.0 g were used in the current study as an experimental animal model for the induction of LPS neurotoxicity, as previously mentioned in Refs. [14–16]. Mice were obtained from the National Research Center at Cairo, placed in polyacrylic cages in groups of no more than five, and maintained under standard conditions of 25 °C room temperature, 60% humidity, and 12 h of light and dark cycles. Food and water were provided to animals. All the experimental procedures of the study were approved by the Institutional Animal Care and Use Committee of Beni-Suef University (approval number: BSU-IACUC:022-353).

2.4.2. Experimental design

Mice were randomly distributed into seven equal groups (10 mice per group as previously mentioned in Refs. [17–19]. The groups were divided as follows: The mice in Group I (negative control) were given seven daily doses of 1% Tween 80 solution in 0.9% saline intraperitoneally (i.p.). LPS was dissolved in 1% Tween 80 solution in 0.9% saline, and a dose of dissolved LPS (0.250 mg/kg body weight, i.p. for seven days) was given to induce neurotoxicity in the LPS Group II mice [20]. Mice in Group III (LPS + QUR) were administered LPS as previously described, and after 2 h, they were orally administered 50 mg/kg body weight of herbal QUR dissolved in distilled water for seven days [21]. In the same procedure, the mice in Group IV (LPS + QUR NANO) were administered LPS as previously described, and after 2 h, they were orally given 50 mg/kg body weight of QUR NANO for seven days [22]. The mice in Group V were administered herbal QUR at the same dose and route as the mice in Group III. Group VI mice were administered QUR NANO at the same dose and route as Group IV mice. The mice in Group VII were orally administered PLGA (10 mg/kg body weight) for seven days [23].

Twenty-four hours after the last dose, all animals were subjected to the Y-maze test for assessment of memory function. Mice were then killed by cervical decapitation, and the brains of the animals were divided as follows: four brains/group were kept in 10% formalin solution for the histopathological examination and electron microscopy, and six brains/group were used for the biochemical and genetic analysis.

2.4.3. Y-maze test

The Y-maze test was used to evaluate spatial memory and spontaneous alternation behavior of mice, as previously described [24, 25]. Briefly, a Y-shaped wooden black apparatus with three arms (14 cm high, 5 cm wide, and 25 cm long) was used. The session lasted 8 min and began by placing the mouse in the center of the maze without any enforcement by water, food, or other stimuli. A series of arm entries was recorded for each mouse. The actual alternation was estimated as consecutive entries into the three arms by the mouse, and the maximum alternation number was measured as the total number of arm entries–2. The spontaneous alternation behavior (SAB) % was estimated as actual alternation/maximum alternation × 100.

2.4.4. Histological examination of the brain

The brains of animals were dissected and washed with normal saline. For histopathological examination, all brain samples were fixed in 10% formalin in saline for 48 h, washed for 1 h in running water, and followed by dehydration in graded ethanol (50%, 70%, 95%, and 100%) for 2 h/each. Sections of five μm tissue thickness were sliced, stained with hematoxylin and eosin (H&E), and examined under a light microscope. A histopathologist examined the hippocampus CA1 region, which is mainly responsible for memory function [26,27], to determine the histological lesions among groups.

For H-RTEM images, the pre-fixed samples were cut into 150 μm sections using vibratome sectioning (Leica, Vienna, Austria). H-RTEM images were obtained using a Jeol Jem 2100 HR instrument equipped with electron energy loss spectroscopy (EELS).

2.4.5. Tissue homogenates preparation

Entire brain tissue, as previously mentioned in Refs. [28,29], was used to prepare 10% w/v tissue homogenate in 0.1 M sodium phosphate-buffered saline solution (pH = 7) and homogenized using an Ultra-Turrax T25 homogenizer (USA). The tissue homogenates were centrifuged for 15 min at 3500 rpm, and the supernatants were withdrawn and kept at −80 °C.

2.4.6. Estimation of oxidative stress biomarkers

The concentrations of glutathione (GSH), malondialdehyde (MDA), and catalase (CAT) were measured using kits provided by Bio-Diagnostic (Egypt) based on the manufacturer's instructions.

2.4.7. Measurements of GABA, $A\beta_{42}$, β-secretase and iNOS levels

GABA, β-secretase, $A\beta_{42}$, and iNOS levels were measured by enzyme-linked immunosorbent assay (ELISA) as follows: GABA by mouse gamma-aminobutyric acid ELISA kit, MyBioSource, USA, β-secretase by mouse β-secretase ELISA kit, MyBioSource, USA, $A\beta_{42}$ by mouse amyloid beta peptide 1–42 ELISA kit, MyBioSource, USA, and iNOS by mouse iNOS ELISA kit, Abcam, U.K.

Briefly, brain tissue homogenate samples were added to the appropriate pre-coated wells and incubated at 37 °C for 1 h. After washing with a washing buffer, the labeled specific antibody solution was pipetted and incubated at 37 °C for another hour. Substrate solutions A and B were added into the wells and incubated at 37 °C for 10 min to develop a colored product. The stop solution was finally added, and the optical density of the developed color was measured at 450 nm by a microplate reader (SunriseTM, TECAN, Switzerland).

2.4.8. Measurement of AChE activity

An aliquot of the brain tissue homogenate was diluted at a ratio of 1:10 for the AChE assay using a QuantiChromTM acetylcholinesterase assay kit from BioAssay Systems (USA). Briefly, the assay depends on an improved Ellman method [30] in which AChE produces thiocholine that interacts with 5,5′-dithiobis (2-nitrobenzoic acid) to produce a colored product directly proportional to the AChE in the sample. Ten μl of each sample was added to the plate wells, and 190 μl of working reagent was added and mixed. The intensity of the produced color was measured kinetically at 412 nm at 2 and 10 min using a microplate reader (SunriseTM, TECAN, Switzerland).

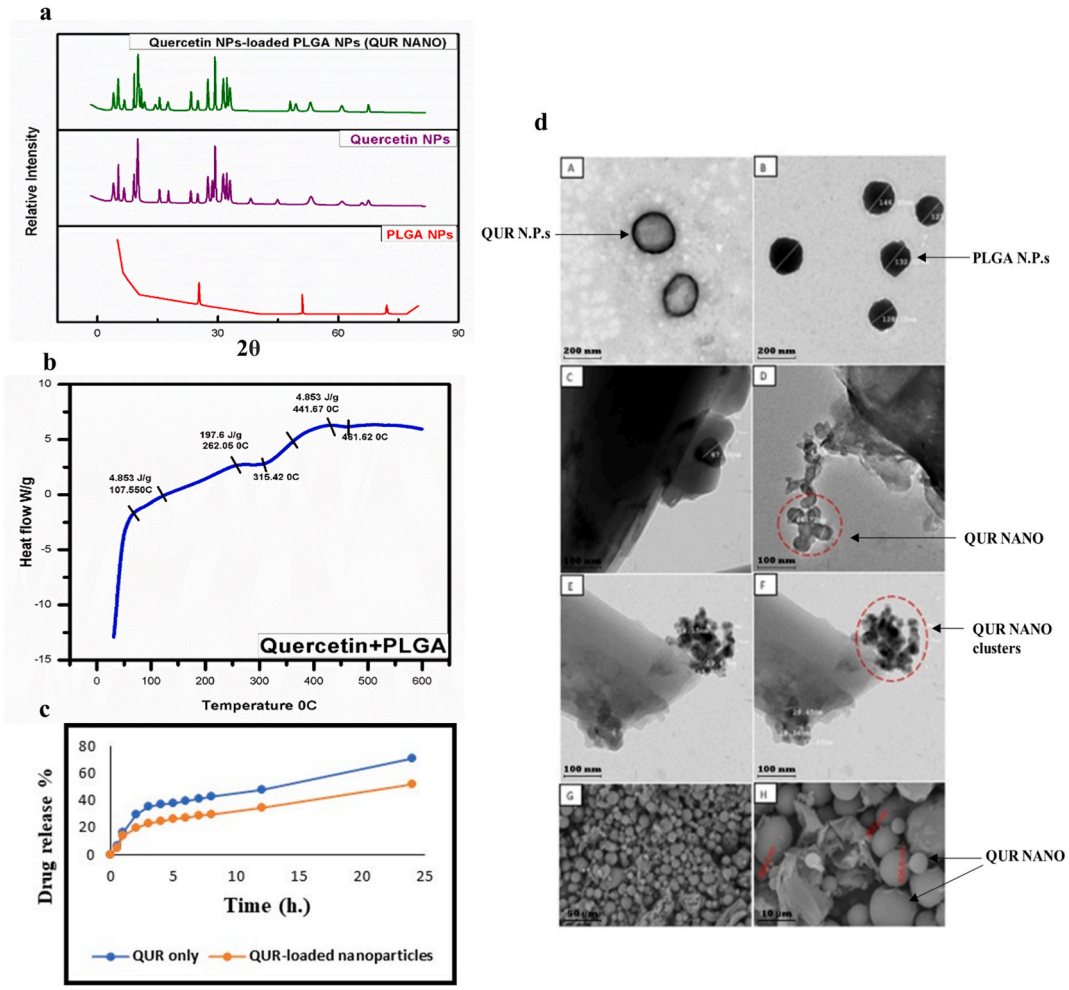

Fig. 1. Characterization and morphology of QUR NANO formulation. (a) The XRD patterns of PLGA, QUR, and QUR NANO. The diffracted peaks of the spectra exhibited sluggish differences in relative intensity, position, and shape over a 2 Theta range, demonstrating the success of the QUR loading process. (b) The DSC thermogram of QUR NANO. (c) *In vitro* drug release of QUR and QUR-loaded nanoparticles. (d) Morphology of QUR NANO formulation showing the following: (A) QUR N.P.s with uniform and spherical shape. (B) PLGA N.P.s with semi-spherical and irregular shape (C–F) H-RTEM images reveal the morphology of QUR NANO, showing clusters of spherical patterns. (G&H) FESEM images show the QUR NANO with a smooth surface area and lacking size uniformity.

2.4.9. Quantitative real time-polymerase chain reaction (qRT-PCR)

The *Nrf2* and *HO-1* gene expression was determined using the qRT-PCR technique. Total RNA from the brain tissue samples was extracted using the RNeasy kit from QIAGEN, Germany, and then reverse-transcribed into cDNA by QuantiTect Reverse Transcription Kit from QIAGEN, Germany. Five μg of single-strand cDNA was used in a 25 μl mixture of 12.5 μl 2x SYBR Green PCR Master Mix (Applied Biosystems, CA, USA) and 200 ng of each primer:

HO-1: Forward 5′-CACGCATATACCCGCTACCT-3′,
Reverse 5′-CCAGAGTGTTCATTCGAGCA -3′, (NM_010442.2) [31].
Nrf2: Forward 5′-TACTCCCAGGTTGCCCACA-3′,
Reverse 5′- CATCTACAAACGGGAATGTCTGC-3′, (AH006764.2) [32].
β-actin: Forward 5′- TCAGGTCATCACTATCGGCAAT-3′,
Reverse 5′- AAGAAAGGGTGTAAAACGCA- 3′, (NM_007393.5) [33].

PCR was performed under the conditions of 95 °C for 10 min, followed by 94 °C for 15 s, and finally 60 °C for 1 min, using the StepOnePlus Real-Time PCR system (Applied Biosystems, USA). Data were analyzed and quantified using the ABI Prism 7500 sequence detection system (P.E. Biosystems, CA). The comparative threshold cycle method [34] was employed to calculate *Nrf2* and *HO-1* gene expression, with all Ct values normalized to the reference gene, β-actin, as follows:

$\Delta Ct = Ct \text{ of the target gene} - Ct \text{ of the reference } (\beta\text{-actin}) \text{ gene}$

$\Delta\Delta Ct = \Delta Ct \text{ of treated sample} - \Delta Ct \text{ of untreated sample (negative control).}$

$\text{Fold change of target gene} = 2^{-\Delta\Delta Ct}$

2.5. Statistical analysis

The mean ± standard error (SE) was used to present all data. Statistical analyses were performed using SPSS software (IBM, USA). The ANOVA test was used to elucidate the significance among groups, and the Tukey post-hoc test was used to compare mean values pairwise. Differences among groups that are less than 0.05 were considered significant and expressed as small letters (a–f) above the columns for each comparison.

3. Results

3.1. Design and characterization of QUR NANO

The EE and DL of QUR NANO were 92.07 ± 3.21% and 4.62 ± 0.55, respectively. The XRD patterns of PLGA, QUR, and QUR NANO are shown in Fig. 1a. The results demonstrated no prominent peaks in the diffraction pattern of PLGA polymer. However, three peaks with low signal intensities of 26.9°, 50.38°, and 65.66° were detected at 2 Thetas, which indicate less periodicity, low ordering of the hkl planes, and low electron density, confirming low crystallinity of the PLGA polymer. The XRD spectrum of QUR had peaks at 7.8°, 8.6°, 9.6°, 11.3°, 12.1°, 13.5°, 15.5°, 22.1°, 23.7°, 25.1°, 26.3°, 27.1°, 28.4°, 37.4°, and 40.8°. There was a high basal diffraction peak with 100% relative intensity at 13.6° diffraction angle, 6.77 Å. d-spacing, and 485.6 Å. crystallite size. This result reflects QUR loading on the PLGA N.P.s (Fig. 1a).

The differential scanning calorimetry (DSC) curves showed that thermal processes occurred at an onset temperature of 262.05 °C ($D = 197.6\ J \bullet g^{-1}$). An endothermic event at 315.42 °C was found, which was attributed to the loss of volatile constituents like water (Fig. 1b).

The percentages of pure QUR and QUR released from PLGA are presented in Fig. 1c. The release of QUR from nanoparticles was slow after 24 h. On the other side, the release of pure QUR was faster than QUR-loaded PLGA. QUR and QUR-loaded PLGA achieved 70.7% and 51.9% release, respectively, in phosphate buffer at 24 h.

3.2. Morphology of QUR-loaded PLGA nanoparticles

The H-RTEM image of QUR N.P.s, as shown in Fig. 1d, depicts the presence of discrete, uniform, and spherical nanoparticles. No signs of coalescence or aggregation were observed, indicating the stability of the prepared N.P.s. In contrast, the PLGA N.P.s displayed a semi-spherical shape with an irregular shape and an average size of approximately 130 nm. Remarkably, the QUR NANO showed clusters of spherical patterns with an average size of 50 nm. The images displayed two diverse signal intensities (black and gray) caused by varying attenuation of the incident electron beam on the QUR NANO. This attenuation depends on the difference in the electron densities of QUR and PLGA.

Concerning FESEM, a powder sample of QUR NANO was spread on a stub and sputtered with gold to inhibit charging and improve the secondary electron signal required for topographic imaging in FESEM. QUR NANO exhibited particles with smooth surface area and lacking uniformity in size as shown in Fig. 1d (G&H).

3.3. QUR NANO preserved the brain histoarchitecture and improved the cognition of mice

Histopathological examination of the brain hippocampal CA1 region by H&E staining demonstrated that the LPS group exhibited degeneration and congestion signs compared to the negative control group, which showed a normal granular layer and cells. Notably, the LPS + QUR and LPS + QUR NANO groups showed less vascular degeneration than the LPS group did. The QUR, QUR NANO, and PLGA groups showed nearly normal hippocampal tissue (Fig. 2A).

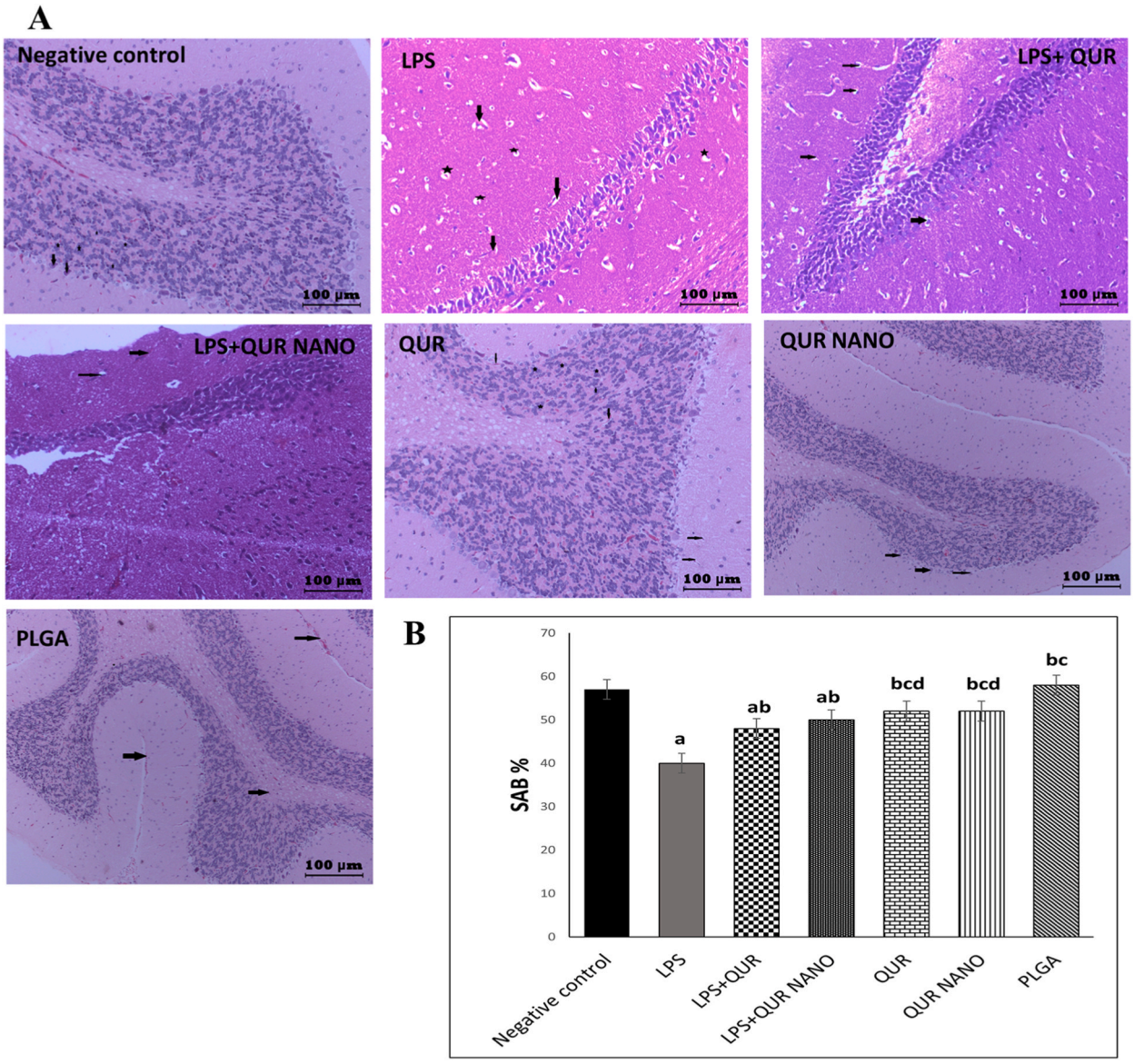

Fig. 2. Effect of QUR NANO on the brain histopathological alterations and memory function. (A) The hippocampal CA1 regions of the examined groups were stained with H&E to reveal the following histological features: The negative control group showed a hippocampal region with normal gray matter, normal Purkinje cells (arrow), and nearly normal white matter (star). The LPS group showed a hippocampal region with pre-vascular edema (arrow) and pre-cellular edema (star), with nearly normal white matter. The LPS + QUR group showed a hippocampal region with a normal granular layer and mild edema in the white matter (arrow). The LPS + QUR NANO group showed a normal hippocampal region with slight vascular degeneration (arrow) and nearly normal cells. The QUR group showed a normal hippocampal region with nearly normal vasculature (arrow) and nearly normal cells (star). The QUR NANO group showed a normal hippocampal region with normal Purkinje cells (arrow). The PLGA group showed a normal hippocampal region in the gray matter, with mild congestion in a few areas (arrow). Scale bar = 100 µm. (B) Column figure shows the percentage of spontaneous alternation behavior (SAB %) in the Y-maze test among the control negative, LPS, LPS + QUR, LPS + QUR NANO, QUR, QUR NANO, and PLGA groups. The SAB % was calculated as the actual alternation/maximum alternation × 100. N = 10 animals/group. a: significant value versus the negative control group, b: significant value versus the LPS group, c: significant value versus the LPS + QUR group, d: significant value versus the LPS + QUR NANO group.

We used the Y-maze behavioral test to assess the spatial memory of mice, and we found a significant decrease in the spontaneous alternation behavior (SAB) in the LPS group to 40% compared to 57% of the negative control group. Remarkably, the administration of herbal QUR or QUR NANO with LPS caused significant increases in SAB to 48% and 50%, respectively, compared to the LPS group. Administration of QUR, QUR NANO, or PLGA alone caused no significant differences in SAB compared to the negative control group (Fig. 2B).

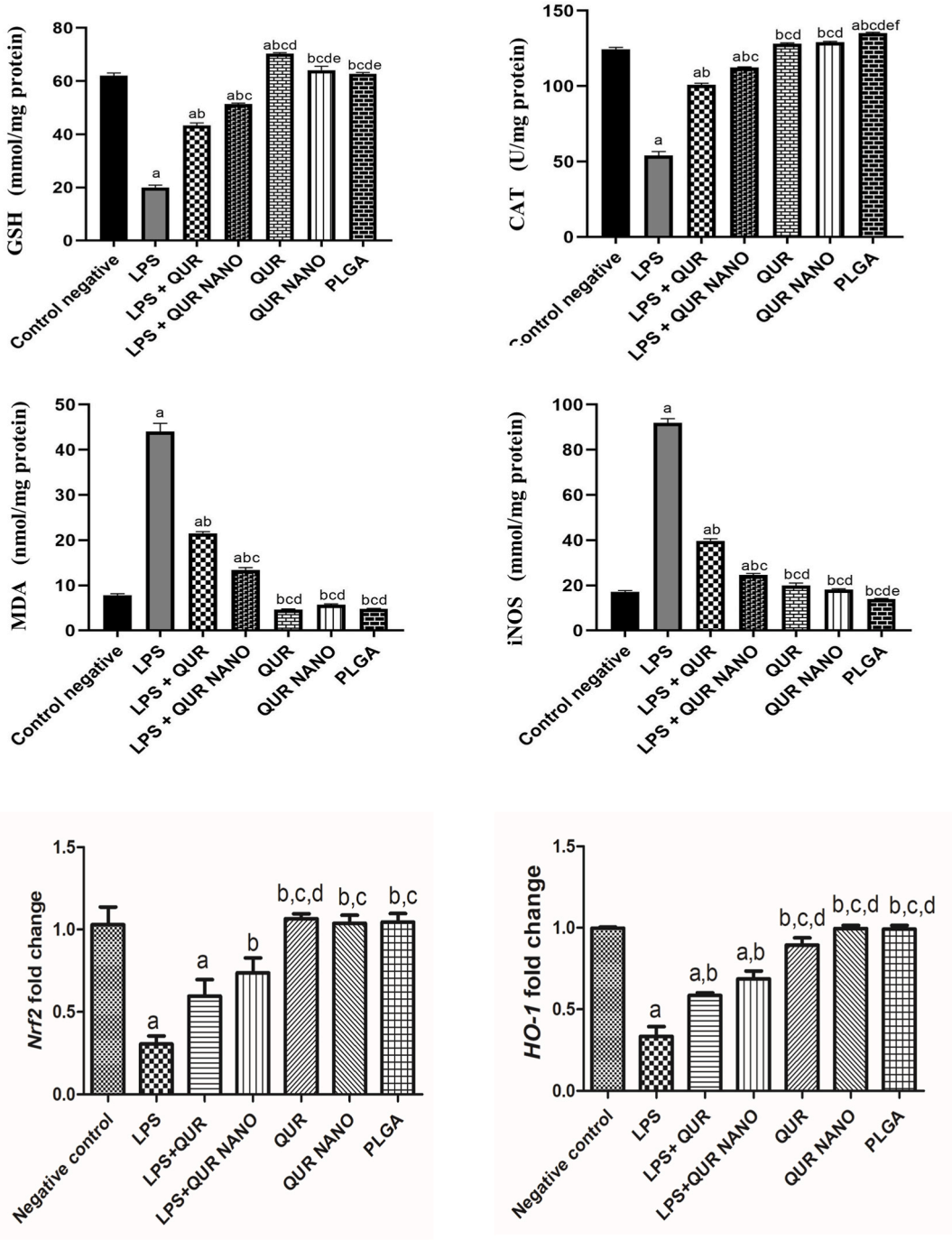

Fig. 3. Effect of QUR NANO formulation on the oxidative stress biomarkers. Column figures show the levels of GSH, CAT, MDA, iNOS, *Nrf2* fold expression, and *HO-1* fold expression in the brain tissue homogenates of the negative control, LPS, LPS + QUR, LPS + QUR NANO, QUR, QUR NANO, and PLGA groups. N = 6 mice/group. a: significant value versus the negative control group, b: significant value versus the LPS group, c: significant value versus the LPS + QUR group, d: significant value versus the LPS + QUR NANO group, e: significant value versus the QUR group, f: significant value versus the QUR NANO group.

Additionally, H-RTEM images of the hippocampus segments in the CA1 region of the LPS + QUR NANO group demonstrated the distribution of QUR NANO into the cytoplasm, indicating that endocytosis is the primary mode of cellular uptake. Moreover, preserving the inner and outer mitochondrial membranes and the normal organelle features confirm the inert and safe action of the QUR NANO in brain cells (Fig. S1).

3.4. QUR NANO formulation exhibited an antioxidant effect

The results revealed significant decreases in GSH concentration by 67.7% and CAT activity by 56.6% in the LPS group and significant increases in MDA level by 466.3% and iNOS activity by 437.7%, compared with the negative control group (Fig. 3). Remarkably, the administration of herbal QUR or QUR NANO with LPS significantly increased the GSH level and CAT activity. In contrast, the MDA and iNOS levels were significantly decreased compared to the LPS group. It is worth noting that the observed antioxidant effect of QUR NANO was significantly higher than that of herbal QUR. However, these improvements were still significantly less than those observed in the negative control group (Fig. 3).

On the molecular level, the LPS group exhibited decreased *Nrf2* gene expression to 0.3-fold compared to the negative control group. In contrast, the LPS + QUR NANO group showed significantly increased *Nrf2* gene expression to 0.7-fold (Fig. 3). Similarly, *HO-1* gene

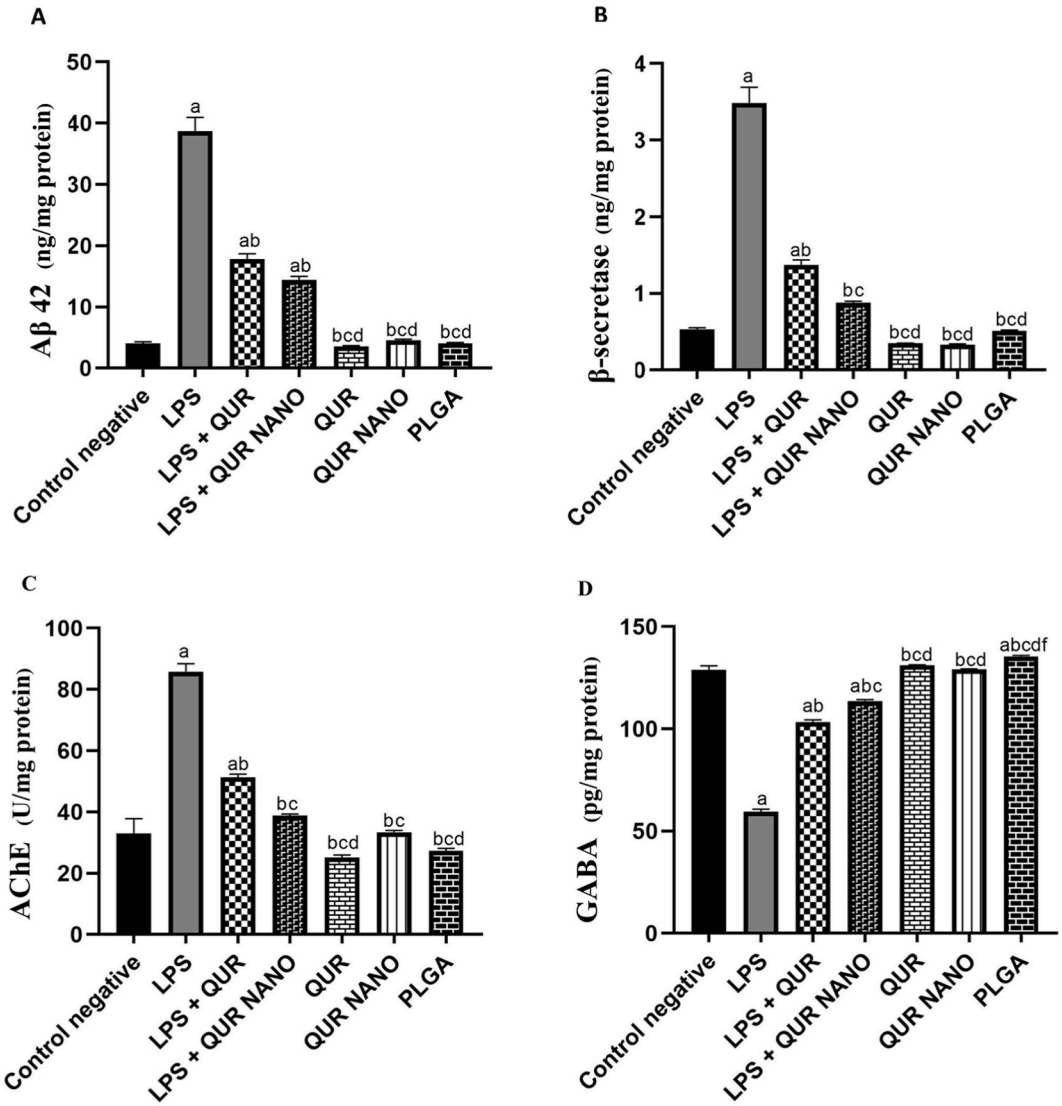

Fig. 4. Effect of QUR NANO formulation on the brain amyloidogenesis and neurotransmission. Column figures show the levels of (A) $A\beta_{42}$, (B) β-secretase, (C) AChE, and (D) GABA in the studied groups. N = 6 mice/group. a: significant value versus the negative control group, b: significant value versus the LPS group, c: significant value versus the LPS + QUR group, d: significant value versus the LPS + QUR NANO group, e: significant value versus the QUR group, f: significant value versus the QUR NANO group.

expression in the LPS group showed a significant decrease to 0.3-fold compared to the negative control group. In contrast, the LPS + QUR and LPS + QUR NANO groups showed significantly increased expression of the *HO-1* gene to 0.6 and 0.7 folds, respectively (Fig. 3). There were no significant differences in *Nrf2* or *HO-1* gene expression of the herbal QUR, QUR NANO, and PLGA groups when compared to the negative control group.

3.5. QUR NANO formulation prevented brain amyloidogenesis and preserved neurotransmission

The LPS group exhibited a significant elevation in $A\beta_{42}$ level compared to the negative control group (38.7 vs. 4.0) and a significant elevation in β-secretase level compared with the negative control group (3.5 vs 0.5). However, the LPS + QUR and LPS + QUR NANO groups revealed significantly decreased $A\beta_{42}$ and β-secretase levels compared to the LPS group. No significant differences in $A\beta_{42}$ or β-secretase levels were detected when the groups of herbal QUR, QUR NANO, and PLGA were compared to the negative control group (Fig. 4A and B).

Our results also revealed an increase in AChE activity by 160.6% in the LPS group compared to the negative control group. However, the LPS + QUR and LPS + QUR NANO groups showed decreased AChE activity compared with the LPS group (Fig. 4C). However, the LPS group showed a 53.9% decrease in GABA levels compared to the negative control group. The LPS + QUR and LPS + QUR NANO groups exhibited increased GABA levels compared to the LPS group (Fig. 4 D). The effect of the LPS + QUR NANO group on preserving AChE and GABA neurotransmitters was significantly better than that of the LPS + QUR group.

4. Discussion

The current research addresses a serious neuroinflammatory condition, introduces an innovative drug delivery method, offers new therapeutic strategies, and sheds light on several molecular mechanisms in the cell.

Our findings demonstrated low crystallinity of the PLGA polymer, where the depicted spectrum matched that of Wenrui et al. [35]. The XRD spectrum of QUR showed similar peaks to those observed in the study by Abd El-Rahmanand et al.; however, they were in slightly different positions [11]. On the other hand, our results about the QUR NANO disagreed with those of M. Giannouli et al., who reported that the XRD pattern of QUR-loaded PLGA nanoparticles showed no QUR peaks, claiming that QUR was dispersed in a non-crystalline form within the polymeric matrix of PLGA [36]. In our study, we noticed the disappearance of the PLGA peaks, which indicated distortion of the crystalline structure, at least in some specific directions. It is known that all diffracting lattice planes should be parallelly aligned to the sample surface to contribute to the diffraction pattern. If this condition is not fulfilled, one does not see any intensity. Another reason for the disappearance of the PLGA peaks is that the planes do not meet Bragg's law conditions for diffraction. In addition, low concentration is a key factor for missing peaks because, at low concentrations, the low-intensity reflections are indistinguishable from noise [37]. Another explanation could be the interaction between the low crystallinity of PLGA and the high crystallinity of QUR.

In the current study, there was a decrease in the size of QUR NANO compared to QUR N.P.s and PLGA N.P.s because we used the emulsification diffusion method in the synthesis of QUR NANO. This method involves neutral, anionic, and cationic charges across the surface of dispersed oil droplets, which may be a critical factor in reducing the size of synthesized nanoparticles.

It is widely known that LPS exposure contributes to cognitive decline and complex behavioral patterns, such as reduction in weight, locomotion, and exploration [38]. The current results showed significant memory decline and brain histological lesions in the LPS group, consistent with a previous study [39].

Notably, LPS exposure promotes ROS production and enhances lipid peroxidation in microglia [40]. Our results demonstrated that LPS exposure resulted in increased MDA and iNOS levels and decreased GSH and CAT levels, reflecting severe oxidative stress consistently with previous studies [39,41]. However, the administration of QUR and QUR NANO protected from the LPS-induced oxidative stress and restored the cellular oxidative defence. A strong relationship between the chemical structure of QUR and its antioxidant effect has been previously attributed to the catechol group and OH group at C-3, which have the ideal organization allowing for free radical scavenging [42]. Previous in vitro studies using blood-brain barrier (BBB) models have indicated that QUR successfully penetrates the BBB and exerts anti-inflammatory actions on brain cells [43]. Additionally, QUR nanoparticles have negative surface charges, which enable the entry of these nanoparticles into neurons by forming nanopores faster than herbal QUR [9]. Our findings showed that the neuroprotective effect of QUR NANO was significantly greater than that of the herbal QUR. A possible explanation might be the small size of QUR NANO that facilitates reaching the cells and the high surface area that enhances the therapeutic effect.

Our study found that QUR administration increased *Nrf2* expression in the brain cells. Consistent with our results, other studies demonstrated that QUR stimulates Nrf2 activation and enhances the transcription of a broad range of antioxidant genes [44,45]. Moreover, our finding that QUR increased *HO-1* expression corroborates the results reported by Sun et al. that QUR induced the transcriptional and translational expression of *HO-1* in a dose- and time-dependent manner in microglia [46]. Notably, oxidative stress stimulates β-secretase activity and $A\beta_{42}$ overproduction [47]. The current study found that QUR effectively decreased β-secretase activity and $A\beta_{42}$ levels in brain tissues, indicating its ability to penetrate the blood-brain barrier, consistent with a previous study [43].

We found that both herbal QUR and QUR NANO significantly decreased AChE activity compared to the LPS group. Our results are consistent with those of Sriraksa et al., who reported that a high QUR dose significantly reduced AChE activity in hippocampal tissue homogenates [48]. This enzyme inhibition is explained by the ability of OH groups of QUR to form hydrogen bonds with critical residues found at the active site of AChE to inhibit its activity [49].

Our findings that the LPS group showed significantly decreased GABA concentrations support the correlation between LPS-induced

neuroinflammation and decreased GABA concentrations [50]. Although there are conflicting results in the literature, most studies suggest that increasing GABA concentration is associated with anti-inflammatory effects via reducing the production of pro-inflammatory cytokines [51]. In our study, the administration of herbal QUR and QUR NANO increased GABA concentrations and reversed LPS-induced toxic effects, consistent with another study [52].

One of the limitations of our study is that the precise mechanisms by which QUR reduced β-secretase and AChE activities were not examined.

Future research should focus on optimizing nanoparticle design and conducting translational studies to evaluate the feasibility of this approach in humans. The effect of QUR on tau protein phosphorylation, the other important contributor to Alzheimer's disease, should also be addressed. This work has the potential to pave the way for novel treatments that address multifaceted aspects of neuroinflammatory conditions associated with memory decline and oxidative stress, such as Alzheimer's disease.

5. Conclusion

The QUR-loaded nanoparticles exhibited protective effects against LPS-induced neurotoxicity in mice by preserving the brain histoarchitecture and memory function, decreasing amyloidogenesis, maintaining neurotransmission, scavenging against oxidative stress, and upregulation the *Nrf2/HO-1* gene expression. The neuroprotective effect of the QUR-loaded nanoparticles was significantly greater than that of herbal QUR.

Ethics statement

All the experimental procedures of the study were approved by the Institutional Animal Care and Use Committee of Beni-Suef University (approval number: BSU-IACUC:022-353).

Funding

This study was supported by individual funding.

Availability of data and material

Data supporting the findings of this study are available in the article or supplementary materials.

CRediT authorship contribution statement

Rasha M. Hussein: Conceptualization, Supervision, Validation, Visualization, Writing – review & editing. **Mohamed A. Kandeil:** Conceptualization, Supervision, Visualization, Writing – review & editing. **Hatem M. Soliman:** Data curation, Formal analysis, Investigation, Methodology, Resources, Writing – original draft. **Ahmed A.G. El-Shahawy:** Methodology, Supervision, Validation, Writing – review & editing, Conceptualization.

Declaration of competing interest

The authors declare that they have no known competing financial interests or personal relationships that could have appeared to influence the work reported in this paper.

Acknowledgements

We thank members of the Materials Science and Nanotechnology Department, PSAS, Beni-Suef University, for supporting the preparation of nanomaterials and Prof. Dr. Mahmoud El-Begawy (Department of Histopathology, Faculty of Veterinary Medicine, Beni-Suef University) for his technical assistance.

Appendix A. Supplementary data

Supplementary data to this article can be found online at https://doi.org/10.1016/j.heliyon.2023.e23527.

References

[1] F. Jiao, Z. Gong, The beneficial roles of SIRT1 in neuroinflammation-related diseases, Oxid. Med. Cell. Longev. 2020 (2020).
[2] M.R. Elmore, A.R. Najafi, M.A. Koike, et al., Colony-stimulating factor 1 receptor signaling is necessary for microglia viability, unmasking a microglia progenitor cell in the adult brain, Neuron 82 (2014) 380–397.
[3] M. Murphy, LeVine 3rd, H., 2010. Alzheimer's disease and the amyloid-beta peptide, J. Alzheimers Dis. 19 (2010) 311–323.

[4] L.G. Costa, J.M. Garrick, P.J. Roquè, C. Pellacani, Mechanisms of neuroprotection by quercetin: counteracting oxidative stress and more, Oxid. Med. Cell. Longev. 2016 (2016).
[5] J.A. Alonso-Piñeiro, A. Gonzalez-Rovira, I. Sánchez-Gomar, J.A. Moreno, M.C. Durán-Ruiz, Nrf2 and heme oxygenase-1 involvement in atherosclerosis related oxidative stress, Antioxidants 10 (2021) 1463.
[6] Y. Tian, W. Wang, L. Xu, et al., Activation of Nrf2/ARE pathway alleviates the cognitive deficits in PS1V97L-Tg mouse model of Alzheimer's disease through modulation of oxidative stress, J. Neurosci. Res. 97 (2019) 492–505.
[7] Y. Li, J. Yao, C. Han, et al., Quercetin, inflammation and immunity, Nutrients 8 (2016) 167.
[8] S.-L. Hwang, P.-H. Shih, G.-C. Yen, Neuroprotective effects of citrus flavonoids, J. Agric. Food Chem. 60 (2012) 877–885.
[9] F. Ghaffari, A.H. Moghaddam, M. Zare, Neuroprotective effect of quercetin nanocrystal in a 6-hydroxydopamine model of Parkinson disease: biochemical and behavioral evidence, Basic Clin. Neurosci. 9 (2018) 317.
[10] M.F. Manzoor, A. Hussain, A. Sameen, et al., Novel extraction, rapid assessment and bioavailability improvement of quercetin: a review, Ultrason. Sonochem. 78 (2021), 105686.
[11] S.N. Abd El-Rahmanand, S. Suhailah, Quercetin nanoparticles: preparation and characterization, Indian J. Drugs 2 (2014) 96–103.
[12] X. Zhu, X. Zeng, X. Zhang, et al., The effects of quercetin-loaded PLGA-TPGS nanoparticles on ultraviolet B-induced skin damages in vivo, Nanomed. Nanotechnol. Biol. Med. 12 (2016) 623–632.
[13] A. Halder, P. Mukherjee, S. Ghosh, S. Mandal, U. Chatterji, A. Mukherjee, Smart PLGA nanoparticles loaded with Quercetin: cellular uptake and in-vitro anticancer study, Mater. Today: Proc. 5 (2018) 9698–9705.
[14] J.-B. Kang, D.-J. Park, M.-A. Shah, M.-O. Kim, P.-O. Koh, Lipopolysaccharide induces neuroglia activation and NF-κB activation in cerebral cortex of adult mice, Lab. Animal Res. 35 (2019) 19.
[15] R. Ullah, G. Ali, A. Baseer, et al., Tannic acid inhibits lipopolysaccharide-induced cognitive impairment in adult mice by targeting multiple pathological features, Int. Immunopharm. 110 (2022), 108970.
[16] C.-H. Yeh, L.-P. Hsieh, M.-C. Lin, et al., Dexmedetomidine reduces lipopolysaccharide induced neuroinflammation, sickness behavior, and anhedonia, PLoS One 13 (2018), e0191070.
[17] J. Zhao, W. Bi, S. Xiao, et al., Neuroinflammation induced by lipopolysaccharide causes cognitive impairment in mice, Sci. Rep. 9 (2019) 5790.
[18] A. Haj-Mirzaian, K. Ramezanzadeh, A. Tafazolimoghadam, et al., Protective effect of minocycline on LPS-induced mitochondrial dysfunction and decreased seizure threshold through nitric oxide pathway, Eur. J. Pharmacol. 858 (2019), 172446.
[19] L. Ma, J. Zhang, Y. Fujita, et al., Effects of spleen nerve denervation on depression–like phenotype, systemic inflammation, and abnormal composition of gut microbiota in mice after administration of lipopolysaccharide: a role of brain–spleen axis, J. Affect. Disord. 317 (2022) 156–165.
[20] Y.-J. Lee, D.-Y. Choi, I.S. Choi, et al., Inhibitory effect of 4-O-methylhonokiol on lipopolysaccharide-induced neuroinflammation, amyloidogenesis and memory impairment via inhibition of nuclear factor-kappaB in vitro and in vivo models, J. Neuroinflammation 9 (2012) 1–19.
[21] A. Kale, Pişkin Ö, Y. Baş, et al., Neuroprotective effects of Quercetin on radiation-induced brain injury in rats, J. Radiat. Res. 59 (2018) 404–410.
[22] E.A. Sánchez-Jaramillo, L.E. Gasca-Lozano, J.M. Vera-Cruz, et al., Nanoparticles formulation improves the antifibrogenic effect of quercetin on an adenine-induced model of chronic kidney disease, Int. J. Mol. Sci. 23 (2022) 5392.
[23] S.M. Navarro, S. Swetledge, T. Morgan, et al., Biodistribution of orally administered poly (lactic-co-glycolic) acid nanoparticles for 7 days followed by 21 day recovery in F344 rats, NanoImpact 5 (2017) 1–5.
[24] A.-K. Kraeuter, P.C. Guest, Z. Sarnyai, The Y-maze for assessment of spatial working and reference memory in mice, in: Pre-clinical Models 105-111, Springer, 2019.
[25] R.M. Hussein, W.R. Mohamed, H.A. Omar, A neuroprotective role of kaempferol against chlorpyrifos-induced oxidative stress and memory deficits in rats via GSK3β-Nrf2 signaling pathway, Pestic. Biochem. Physiol. 152 (2018) 29–37.
[26] Y.L. Rao, B. Ganaraja, B. Murlimanju, T. Joy, A. Krishnamurthy, A. Agrawal, Hippocampus and its involvement in Alzheimer's disease: a review, 3 Biotech 12 (2022) 55.
[27] J.L. Voss, D.J. Bridge, N.J. Cohen, J.A. Walker, A closer look at the hippocampus and memory, Trends Cognit. Sci. 21 (2017) 577–588.
[28] R.M. Hussein, A.M. Youssef, M.K. Magharbeh, et al., Protective effect of Portulaca oleracea extract against lipopolysaccharide-induced neuroinflammation, memory decline, and oxidative stress in mice: potential role of miR-146a and miR-let 7, J. Med. Food 25 (2022) 807–817.
[29] W.A. Khallaf, B.A. Messiha, A.M. Abo-Youssef, N.S. El-Sayed, Protective effects of telmisartan and tempol on lipopolysaccharide-induced cognitive impairment, neuroinflammation, and amyloidogenesis: possible role of brain-derived neurotrophic factor, Can. J. Physiol. Pharmacol. 95 (2017) 850–860.
[30] D. Dingova, J. Leroy, A. Check, V. Garaj, E. Krejci, A. Hrabovska, Optimal detection of cholinesterase activity in biological samples: modifications to the standard Ellman's assay, Anal. Biochem. 462 (2014) 67–75.
[31] W-w Xing, M-j Zou, S. Liu, et al., Hepatoprotective effects of IL-22 on fulminant hepatic failure induced by d-galactosamine and lipopolysaccharide in mice, Cytokine 56 (2011) 174–179.
[32] J. Xu, Y. Zhang, G. Ren, et al., Inhibitory effect of delphinidin on oxidative stress induced by H2O2 in HepG2 cells, Oxid. Med. Cell. Longev. 2020 (2020).
[33] J. Ren, C. Fan, N. Chen, J. Huang, Q. Yang, Resveratrol pretreatment attenuates cerebral ischemic injury by upregulating expression of transcription factor Nrf2 and HO-1 in rats, Neurochem. Res. 36 (2011) 2352–2362.
[34] K.J. Livak, T.D. Schmittgen, Analysis of relative gene expression data using real-time quantitative PCR and the 2− ΔΔCT method, Methods 25 (2001) 402–408.
[35] W. Wang, R. Zhu, Q. Xie, et al., Enhanced bioavailability and efficiency of curcumin for the treatment of asthma by its formulation in solid lipid nanoparticles, Int. J. Nanomed. 7 (2012) 3667.
[36] M. Giannouli, V. Karagkiozaki, F. Pappa, I. Moutsios, C. Gravalidis, S. Logothetidis, Fabrication of quercetin-loaded PLGA nanoparticles via electrohydrodynamic atomization for cardiovascular disease, Mater. Today: Proc. 5 (2018) 15998–16005.
[37] R. Naorem, A. Gupta, S. Mantri, et al., A critical analysis of the X-ray diffraction intensities in concentrated multicomponent alloys, Int. J. Mater. Res. 110 (2019) 393–405.
[38] J.W. Lee, Y.K. Lee, D.Y. Yuk, et al., Neuro-inflammation induced by lipopolysaccharide causes cognitive impairment through enhancement of beta-amyloid generation, J. Neuroinflammation 5 (2008) 1–14.
[39] R.M. Hussein, A.M. Youssef, M.K. Magharbeh, et al., Protective effect of portulaca oleracea extract against lipopolysaccharide-induced neuroinflammation, memory decline, and oxidative stress in mice: potential role of miR-146a and miR-let 7, J. Med. Food (2022).
[40] J. Park, J.-S. Min, B. Kim, et al., Mitochondrial ROS govern the LPS-induced pro-inflammatory response in microglia cells by regulating MAPK and NF-κB pathways, Neurosci. Lett. 584 (2015) 191–196.
[41] K. Noworyta-Sokołowska, A. Górska, K. Gołembiowska, LPS-induced oxidative stress and inflammatory reaction in the rat striatum, Pharmacol. Rep. 65 (2013) 863–869.
[42] C.G. Heijnen, G.R. Haenen, J.A. Vekemans, A. Bast, Peroxynitrite scavenging of flavonoids: structure activity relationship, Environ. Toxicol. Pharmacol. 10 (2001) 199–206.
[43] X. Zhou, G. Li, B. Yang, J. Wu, Quercetin enhances inhibitory synaptic inputs and reduces excitatory synaptic inputs to OFF-and ON-type retinal ganglion cells in a chronic glaucoma rat model, Front. Neurosci. 13 (2019) 672.
[44] M. Kimura, T. Yamamoto, J. Zhang, et al., Molecular basis distinguishing the DNA binding profile of Nrf2-Maf heterodimer from that of Maf homodimer, J. Biol. Chem. 282 (2007) 33681–33690.
[45] P. Yao, A. Nussler, L. Liu, et al., Quercetin protects human hepatocytes from ethanol-derived oxidative stress by inducing heme oxygenase-1 via the MAPK/Nrf2 pathways, J. Hepatol. 47 (2007) 253–261.
[46] G.Y. Sun, Z. Chen, K.J. Jasmer, et al., Quercetin attenuates inflammatory responses in BV-2 microglial cells: role of MAPKs on the Nrf2 pathway and induction of heme oxygenase-1, PLoS One 10 (2015), e0141509.

[47] E. Tamagno, M. Guglielmotto, M. Aragno, et al., Oxidative stress activates a positive feedback between the γ-and β-secretase cleavages of the β-amyloid precursor protein, J. Neurochem. 104 (2008) 683–695.
[48] N. Sriraksa, J. Wattanathorn, S. Muchimapura, S. Tiamkao, K. Brown, K. Chaisiwamongkol, Cognitive-enhancing effect of quercetin in a rat model of Parkinson's disease induced by 6-hydroxydopamine, Evid. Based Complement Alternat. Med. 2012 (2012).
[49] M. Katalinić, G. Rusak, J.D. Barović, et al., Structural aspects of flavonoids as inhibitors of human butyrylcholinesterase, Eur. J. Med. Chem. 45 (2010) 186–192.
[50] T. Crowley, J.F. Cryan, E.J. Downer, O.F. O'Leary, Inhibiting neuroinflammation: the role and therapeutic potential of GABA in neuro-immune interactions, Brain Behav. Immun. 54 (2016) 260–277.
[51] A.K. Bhandage, J.L. Cunningham, Z. Jin, et al., Depression, GABA, and age correlate with plasma levels of inflammatory markers, Int. J. Mol. Sci. 20 (2019) 6172.
[52] S.S. Elblehi, E.M. Abd El-Maksoud, A. Aldhahrani, et al., Quercetin abrogates oxidative neurotoxicity induced by silver nanoparticles in wistar rats, Life 12 (2022) 578.